Respiratory Motion Guided Four Dimensional Cone Beam Computed Tomography: Encompassing Irregular Breathing

Ricky T O'Brien[1], Benjamin J Cooper[1,2], John Kipritidis[1], Chun-Chien Shieh[1,3] and Paul J Keall[1]

[1] Radiation Physics Laboratory, Sydney Medical School, The University of Sydney, NSW 2006, Australia.

[2] Department of Medical Physics, The Canberra Hospital, ACT 2605, Australia.

[3] Institute of Medical Physics, School of Physics, The University of Sydney, NSW 2006, Australia.

E-mail: `ricky.obrien@sydney.edu.au`

Abstract. Four dimensional cone beam computed tomography (4DCBCT) images suffer from angular under sampling and bunching of projections due to a lack of feedback between the respiratory signal and the acquisition system. To address this problem, Respiratory Motion Guided 4DCBCT (RMG-4DCBCT) regulates the gantry velocity and projection time interval, in response to the patient's respiratory signal, with the aim of acquiring evenly spaced projections in a number of phase or displacement bins during the respiratory cycle. Our previous study of RMG-4DCBCT was limited to sinusoidal breathing traces. Here we expand on that work to provide a practical algorithm for the case of real patient breathing data. We give a complete description of RMG-4DCBCT including full details on how to implement the algorithms to determine when to move the gantry and when to acquire projections in response to the patient's respiratory signal. We simulate a realistic working RMG-4DCBCT system using 112 breathing traces from 24 lung cancer patients. Acquisition used phase-based binning and parameter settings typically used on commercial 4DCBCT systems (4 minute acquisition time, 1200 projections across 10 respiratory bins), with the acceleration and velocity constraints of current generation linear accelerators. We quantified streaking artefacts and image noise for conventional and RMG-4DCBCT methods by reconstructing projection data selected from an oversampled set of Catphan phantom projections. RMG-4DCBCT allows us to optimally trade-off image quality, acquisition time and image dose. For example, for the same image quality and acquisition time as conventional 4DCBCT approximately half the imaging dose is needed. Alternatively, for the same imaging dose, the image quality as measured by the signal to noise ratio, is improved by 63% on average. C-arm CBCT systems, with an acceleration up to $200^\circ/s^2$, a velocity up to $100^\circ/s$ and the acquisition of 80 projections per second, allow the image acquisition time to be reduced to below 60 seconds. We have made considerable progress towards realising a system to reduce projection clustering in conventional 4DCBCT imaging and hence reduce the imaging dose to the patient.

1. Introduction

The United States Food and Drugs Administration's (FDA's) initiative to reduce unnecessary radiation exposure from medical imaging, Image Wisely and Image Gently‡ are three high profile campaigns to increase public and clinical awareness on the risks and undesirable side effects associated with radiation delivered during medical imaging. In an ideal world, preference would be given to an imaging modality if medically relevant images can be acquired with a lower radiation dose. However, in practice, the financial cost of the imaging modality, the benefit to the patient, the time required to acquire the images, patient discomfort and the imaging dose are all balanced before an imaging modality is selected.

An emerging clinical image guidance strategy for tumour sites affected by respiratory motion is four dimensional cone beam computed tomography (4DCBCT) in which a series of approximately 1200 kilovoltage images, or projections, are used to reconstruct a 3D view of the patient's anatomy (Taguchi 2003), (Sonke et al. 2005). Elekta released 4DCBCT as part of their Symmetry product in 2009 while Varian released 4DCBCT in 2013 as part of their Advanced IGRT package on TrueBeam 2.0. The clinical drivers for 4DCBCT are the desire to obtain, on the day of treatment, information on the average tumour position, the amplitude of the tumour motion, validation of the treatment plan, inter fraction changes in the tumour size and shape and to improve the accuracy of image-guidance (Sweeney et al. 2012). 4DCBCT is also the subject of substantial research and development efforts. A pubmed search of '4d Cone Beam CT' on 18/10/2013 yielded 119 articles, with over half of these articles (63) published in the last 2.5 years indicating substantial growth in the 4DCBCT topic. However, the accumulated radiation dose delivered to a patient from frequent use of 4DCBCT over the course of their treatment can be significant and efforts to reduce the radiation dose from 4DCBCT imaging will have a direct benefit to the patient.

Projection clustering, that is inherent in conventional 4DCBCT techniques, is known to cause streak artefacts and degrade image quality (Leng et al. 2008). This paper is concerned with Respiratory Motion Guided 4DCBCT (RMG-4DCBCT), which is a technique that can be used to reduce projection clustering and improve image quality when acquiring 4DCBCT images. RMG-4DCBCT utilises the real-time respiratory signal enabling two additional degrees of freedom over conventional 4DCBCT: (1) the velocity of the gantry can be varied and (2) the time interval between projections can be varied. Varying the velocity of the gantry and the time interval between projections allows us to improve the angular spacing of projections and to improve the image quality of 4DCBCT images.

In our previous study, (O'Brien et al. 2013), we introduced a mathematical

‡ http://www.fda.gov/Radiation-EmittingProducts/RadiationSafety/RadiationDoseReduction/default.htm, http://www.imagewisely.org/ and http://www.pedrad.org/associations/5364/ig/ respectively. The International Commission on Radiological Protection's (ICRP's) As Low As Reasonably Achievable (ALARA) principle is another campaign to reduce radiation exposure.

framework for the optimisation algorithms that are used to compute the optimal gantry velocity and projection time interval schedule for RMG-4DCBCT. The optimisation algorithms in our previous study were demonstrated only on simulated sinusoidal breathing traces and not real patient breathing data. This article builds on our previous studies by implementing the optimisation into a realistic simulation of a working RMG-4DCBCT software package. We will give complete details on the software system that is used to implement RMG-4DCBCT in a simulated environment. We will introduce the algorithms that are used to determine when to move the gantry, how to move the gantry smoothly and when to acquire a projection. To make the system more realistic we have developed a simulated gantry and a simulated kilovoltage imager and commands are issued to the simulated system. We establish that RMG-4DCBCT is an effective method to reduce projection clustering by performing a realistic simulation of a working RMG-4DCBCT system using 112 breathing traces from 24 lung cancer patients acquired in a previous study (George et al. 2006).

2. Theory

In this section we demonstrate why projection clustering occurs in 4DCBCT and how the algorithms are implemented in an RMG-4DCBCT system.

2.1. 4DCBCT Imaging and Projection Clustering

Modern linear accelerators are equipped with kilovoltage (kV) imagers which are used to position patients for treatment. By rotating the gantry, containing the kV imager and detector, around the patient a series of approximately 1200 images, or projections, can be acquired. We will refer to the kV images as projections throughout the remainder of this paper. The projections are used to reconstruct a three dimensional image, or cone beam computed tomography (CBCT) image, of the patient's anatomy using the Feldkamp-Davis-Kress (FDK) algorithm (Feldkamp et al. 1984). The whole process takes several minutes to acquire the projections necessary to reconstruct a CBCT image of acceptable quality for radiotherapy.

A major problem with CBCT imaging is respiratory motion, which causes artefacts and blurring in the resulting 3D image because the anatomy is continuously moving during the projection acquisition process. To overcome the problems associated with respiratory motion, 4DCBCT techniques have been developed (Taguchi 2003), (Sonke et al. 2005) and commercially released in 2009 by Elekta (Stockholm Sweden). The aim of 4DCBCT imaging is to collect a full set of projections in a number of phase or displacement respiratory bins. Within each respiratory bin there is little anatomical motion so blurring and artefacts in the resulting images are reduced. For example, projections taken at the inhale or exhale limit are allocated to the inhale or exhale limit respiratory bins respectively and are used to reconstruct a 3D image for the corresponding respiratory bin.

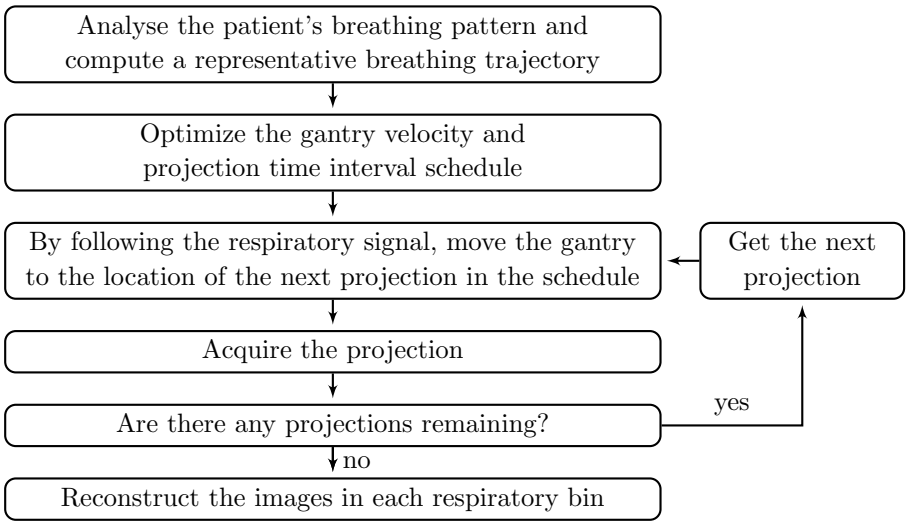

Figure 1. A flowchart showing the main algorithm controlling RMG-4DCBCT.

Common to all current 4DCBCT systems is the use of a constant gantry velocity with a constant projection pulse rate. After the projections have been acquired, they are compared to the recorded respiratory signal and then post-processed into respiratory bins. Throughout the image acquisition process there is no feedback from the respiratory signal to the acquisition system. This leads to a cluster of projections while the breathing signal is in a respiratory bin, followed by a gap as the gantry continues to move while we wait for the respiratory signal to re-enter the respiratory bin. Clustering of projections leads to streak artefacts in the reconstructed images (Leng et al. 2008).

2.2. RMG-4DCBCT

In order to reduce projection clustering there are two additional degrees of freedom used in RMG-4DCBCT. The first degree of freedom allows the velocity of the gantry to be regulated within specified limits on maximum velocity and maximum acceleration. The second degree of freedom allows the time interval between projections to be regulated, i.e. the projections can be brought forward or delayed. These two degrees of freedom allow us to speed up the gantry and delay projections with the aim of improving the angular separation between projections. Figure 1 gives a flowchart for RMG-4DCBCT. We describe each step in the process in more detail, and give implementation details, in the remainder of this section.

2.3. Analyse the patient's breathing pattern and compute a representative breathing trajectory

A respiratory signal can be derived from the projections themselves (Zijp et al. 2004), (Van Herk et al. 2007), (Berbeco et al. 2005), (Kavanagh et al. 2009), (Vergalasova et al. 2012) or from an external respiratory sensor such as the Real-Time Position

Management System (RPM) (Varian Medical Systems, Palo Alto, CA). In this study we use the RPM system which has a frequency of 30Hz because we have a large database of RPM breathing traces from lung cancer patients. We denote the respiratory signal as $R(t_i)$ for $i = 1, 2, \ldots$ where $t_{i+1} - t_i = 33$ms for the RPM system.

The RPM data is sent via serial port to the RMG-4DCBCT software and includes the real-time displacement of a marker block placed on the patients abdomen and a real-time estimate of the patient's breathing phase. In addition to receiving respiratory data directly from the RPM computer an RPM emulator has been developed to read files saved from a previous study and to send the data to the RMG-4DCBCT software via serial port. This allows us to use an RPM signal from data previously recorded for lung cancer patients as if the patient were present.

For the optimisation in the next section a representative breathing trajectory is required. Although the optimisation could be improved with an accurate prediction of the patient's breathing, a highly accurate prediction is both technically difficult and not necessary. To keep the system simple, we monitor 10 breathing cycles, compute the average baseline, phase and range of motion of the respiratory signal, and then use a sine wave for the representative breathing trajectory used to optimize the acquisition schedule.

2.4. Optimize the gantry velocity and projection time interval schedule

Optimising the gantry velocity and projection time interval schedule is achieved using Mixed Integer Quadratic Programming (MIQP) techniques (O'Brien et al. 2013). The method minimises the Root Mean Square (RMS) of the difference between the angular separation and the mean angular separation for projections in the same respiratory bin. Mathematically, the RMS can be defined by assuming that we have N respiratory bins with M_b projections taken in bin b, we let $\theta_{b,l}$ for $b = 1, 2, \ldots, N$ and $l = 1, 2, \ldots, M_b$ be the l^{th} largest gantry angle for the projections taken in respiratory bin b, then the RMS in bin b is

$$RMS_b^2 = \left\{ \sum_{l=1}^{M_b-1} \left(\theta_{b,l+1} - \theta_{b,l} - \Delta\theta_b\right)^2 + \left(2\pi - \left(\theta_{b,M_b} - \theta_{b,0}\right) - \Delta\theta_b\right)^2 \right\} / M_b, \quad (1)$$

where $\Delta\theta_b = 2\pi/M_b$ is the average angular separation between projections. The term in the summation $(\theta_{b,l+1} - \theta_{b,l} - \Delta\theta_b)$ is the angular distance between projections minus the average angular separation. The final term $(2\pi - (\theta_{b,M_b} - \theta_{b,0}) - \Delta\theta_b)$ is the angular separation between the first and last projection minus the average angular separation. The objective function, or RMS, that is minimized is

$$\text{RMS}^2 = \text{Minimise} \sum_{b=1}^{N} RMS_b^2/N, \quad (2)$$

Additional constraints are applied on the maximum velocity and acceleration of the gantry, the minimum time between projections and to ensure that M_b projections are collected in respiratory bin b. We refer to our previous study for more details on the implementation of the optimization algorithms (O'Brien et al. 2013).

For safety reasons, the International Electrotechnical Commission (I.E.C) specifies a maximum velocity of $6^\circ/s$ which is the maximum velocity for most linear accelerators. Values for acceleration have been measured at between $1.8^\circ/s^2$ and $3.2^\circ/s^2$, and deceleration at between $3.4^\circ/s^2$ and $4.3^\circ/s^2$ for the Elekta Synergy linear accelerator (Boylan et al. 2011). Values for acceleration and deceleration for non emergency stops on the Varian Medical Systems TrueBeam are around $12^\circ/s^2$ §. Conventional kilovoltage imagers are capable of acquiring images at a rate of at least 10Hz, so in our optimization we will apply a constraint ensuring that projections are taken at least 100ms apart. At the high end of the acceleration and velocity scale are the C-arm systems that are capable of a velocity of $100^\circ/s$, an acceleration of $200^\circ/s^2$ and a projection pulse rate of 80Hz‖.

A heuristic solution method to the MIQP model that obtains a near optimal gantry velocity and projection time interval schedule in under one second is given by (O'Brien et al. 2013). The output of the optimisation is a sequence of projections points, P_k, containing the representative respiratory signal, R_k, gantry angle, θ_k, and estimated acquisition time, t_k

$$P_k(\theta_k, R_k, t_k) \text{ for } k = 1, 2, \ldots, M,$$

where M is the total number of projections $M = \sum_{b=1}^{N} M_b$.

2.5. Following the respiratory signal and moving the gantry to the location of the next projection in the schedule

The projection sequence points, P_k, are given when projections need to be taken and are separated by a time interval of at least 100ms. To move the gantry smoothly, we need to interpolate between the projection points to obtain a trajectory for the gantry at a resolution of around 10-50ms. There are two parameters that we could use to perform the interpolation: either use time t_k, or, the respiratory signal R_k. Time t_k is a bad choice because the patient's breathing trace will quickly drift away from the representative breathing trace. Projections need to be taken when the respiratory signal is in the correct position, so interpolation is performed using the respiratory signal, R_k. We need to continuously monitor the respiratory signal and trigger projections based on the respiratory signal and not time.

We interpolate using a quadratic function to fit gantry trajectory points, this is schematically depicted in Figure 2. That is, we use the respiratory signal at, R_{k-1}, R_k and R_{k+1} to fit a quadratic curve and interpolate between $(R_{k-1} + R_k)/2 \leq R < (R_{k+1} + R_k)/2$

$$\theta(R) = AR^2 + BR + C \text{ for } (R_{k-1} + R_k)/2 \leq R < (R_{k+1} + R_k)/2,$$

§ Personal communication with Scott Johnson, Sr Manager, Research Collaborations, Varian Medical Systems, 5 September 2012.

‖ http://zeegolab.stanford.edu/

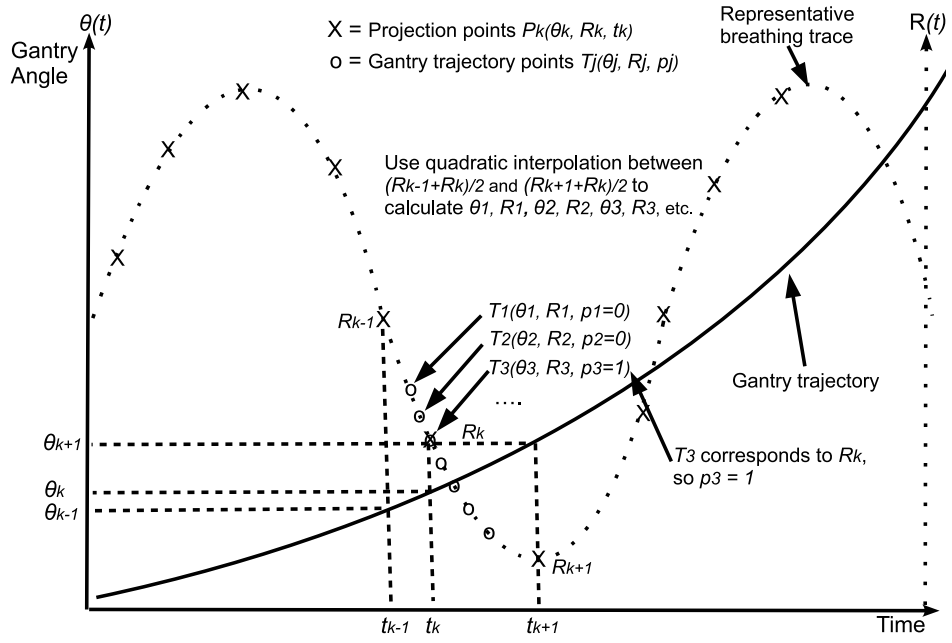

Figure 2. A schematic depicting how the projection points $P_k(\theta_k, R_k, t_k)$ are used to determine the gantry trajectory points $T_j(R_j, \theta_j, p_j)$ between $(R_{k-1} + R_k)/2$ and $(R_{k+1} + R_k)/2$.

where

$$
\begin{aligned}
A = {} & [(\theta_k - \theta_{k-1})(R_{k-1} - R_{k+1}) + (\theta_{k+1} - \theta_{k-1})(R_k - R_{k-1})] \\
& \Big/ \left[(R_{k-1} - R_{k+1})(R_k^2 - R_{k-1}^2) + (R_k - R_{k-1})(R_{k+1}^2 - R_{k-1}^2)\right], \\
B = {} & \left[(\theta_{k+1} - \theta_k) - A(R_{k+1}^2 - R_{k-1}^2)\right] / (R_k - R_{k-1}), \\
C = {} & \theta_{k-1} - AR_{k-1}^2 - BR_{k-1}.
\end{aligned}
$$

We use this equation to compute a sequence of gantry trajectory points, $T_j(R_j, \theta_j, p_j)$ for $j = 1, 2, \ldots$ at a resolution of around 10-50ms. The parameter p_j is 1 if the trajectory point corresponds to a projection point and zero otherwise.

Once we have computed the gantry trajectory points, we use them to move the gantry in response to the patient's real-time respiratory signal. We start with $j = 1$, when the patient's respiratory signal, $R(t)$ is R_1 we move the gantry to θ_1. If a projection is to be taken, i.e. $p_j = 1$, we issue a command to the imager to take a projection. We then set $j = 2, 3, \ldots$ and repeat the process. A flowchart of this process is given in Figure 3 with the details required to wait for $R(t) = R_j$ discussed in the next section.

2.5.1. Predicting the respiratory signal and waiting for $R(t) = R_j$: The gantry trajectory points are at a resolution of 10-50ms while the RPM signal is received at a resolution of 33ms. It is therefore necessary to predict the RPM signal for up to 33ms. For example, assuming phase goes from 0 to 2π, if our next gantry trajectory point

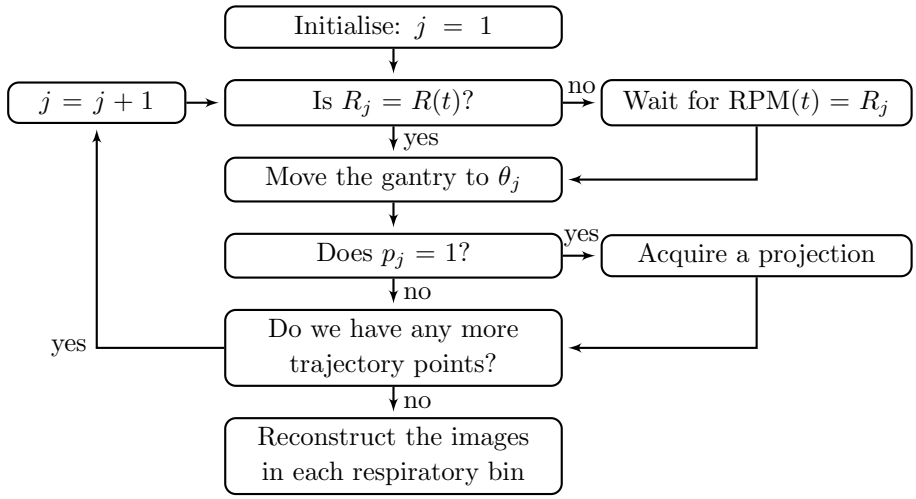

Figure 3. A flowchart showing how to move the gantry to each trajectory point. This algorithm moves the gantry to trajectory points θ_j for $j = 1, 2, \ldots$.

indicates that the gantry should be moved when the phase is 1.025 and the last two RPM signals were 0.9 and 1.0, we expect a phase of 1.025 to occur before we receive the next respiratory signal. With a prediction interval of at most 33ms, we use linear extrapolation to predict the respiratory signal. More complicated algorithms can be used to predict the respiratory signal with reasonable accuracy for intervals between 200-500ms (Krauss et al. 2011).

2.5.2. Prediction errors: Figure 4 is a diagram showing that projections can be taken in the wrong respiratory bin because of errors in predicting the respiratory signal. In Figure 4, a projection is required with a phase of 1.17. We predict that the phase will be 1.17 at 55ms and acquire the projection at this time. However, when we receive the next signal, at 66ms, we find that the prediction was incorrect and the projection was taken in the bin 3 not bin 2. To reduce the occurrence of prediction errors we add a buffer to respiratory bins when optimising the projection schedule so that projections are not taken close to the boundary of a time window. We have found that a 5ms buffer on the respiratory bins is sufficient in most cases.

2.5.3. Large jumps in the real-time phase signal: On our database of breathing traces from lung cancer patients the real-time phase signal contains fast transitions or 'jumps' in the phase. Figure 5 is a screen shot from our RMG-4DCBCT software showing an example of jumps in the real-time phase signal. When a jump occurs the problems mentioned in the previous section are greatly magnified and there is no way of guaranteeing that the projection will be taken in the correct respiratory bin. In the example in Figure 5 the first of the two projections allocated to the pink respiratory bin should have been taken in the preceding respiratory bin. If the imager is capable of a high frame rate, where 4 or 5 projections could be acquired between respiratory

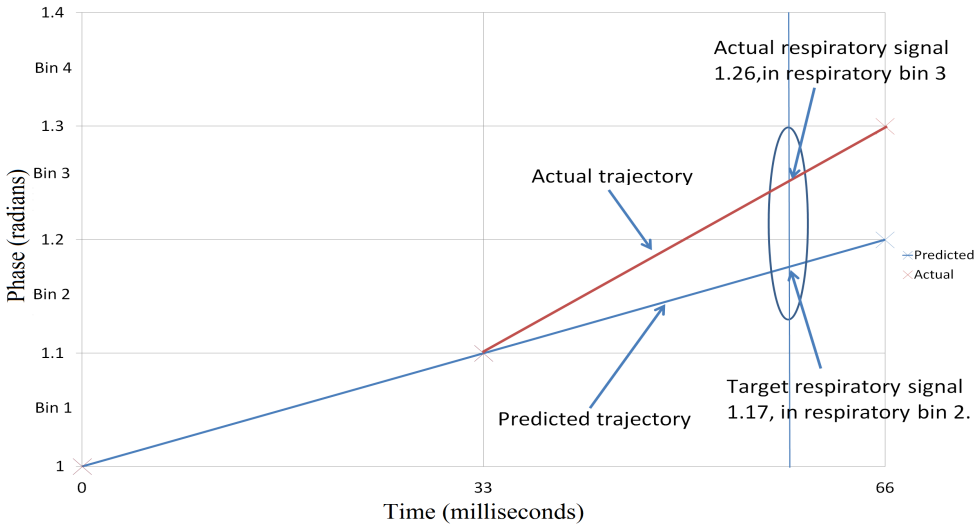

Figure 4. Prediction errors: An RPM signal is received at time 0 and 33ms. A projection is required when the phase is 1.17 which is predicted to occur at 55ms. We issue a command to the kilovoltage imager to acquire a projection at 55ms. However, once we receive the RPM signal at 66ms we find that the projection was actually taken in bin 3, not bin 2.

signals, the quality of the real-time phase signal can be the biggest factor influencing acquisition.

There are two options on what we can do with the projection if a jump occurs:

(i) Allocate the projection to the respiratory bin that the projection was taken (i.e. we allocate both projections in Figure 5 to the pink respiratory bin).

(ii) Because the phase signal is changing rapidly, the resulting projection can be allocated to the target, or expected, respiratory bin (i.e. we allocate the first projection to the blue respiratory bin in Figure 5).

Throughout this study we will use option i because it represents the worst case scenario as far as the angular separation of projections is concerned. Option ii will produce better angular separation between projections, but further studies of clinical images will be needed to assess the impact on image quality.

2.5.4. Alternative phase signals: As an alternative to the phase signal computed by the RPM sensor, we have implemented the method of (Ruan et al. 2009) to compute a real-time phase estimate. To further reduce the high frequency oscillations in the respiratory signal we have also applied a low pass filter to the respiratory data when implementing the Ruan real-time phase estimation.

3. Method

Four different 4DCBCT algorithms have been studied. Figure 6 gives a screen shot from the RMG-4DCBCT software showing the differences between the four 4DCBCT

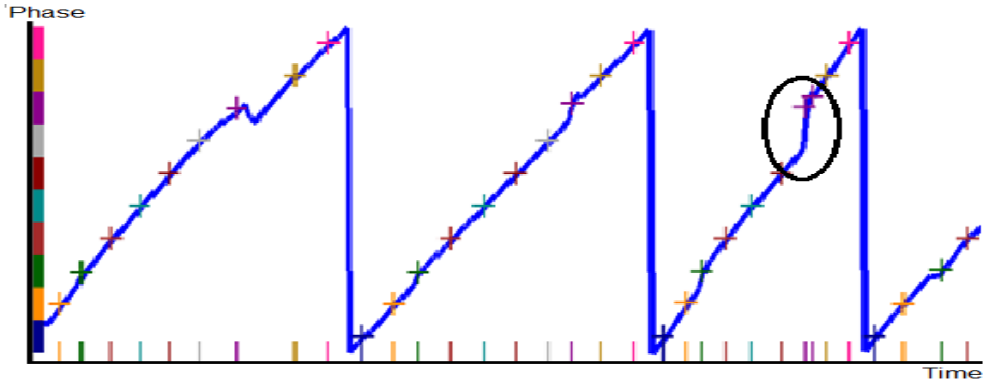

Figure 5. An example of sudden jumps in the RPM phase signal. A screen shot from the RMG-4DCBCT software showing the phase signal over three respiratory cycles (15 seconds). The 10 colours on the left hand side identify the respiratory bins and the crosses correspond to projections taken using RMG-4DCBCT. The area marked with the ellipse shows a region where the respiratory signal suddenly jumps. Also note that the first two breathing cycles exhibit similar, but smaller, jumps.

Table 1. Default parameters used for the four 4DCBCT methods. The relative dose is the radiation dose delivered from the imaging technique relative to conventional 4DCBCT. ω is the average breathing period of the patient.

	Conventional 4DCBCT	RMG-4DCBCT$^{1200}_{240}$	RMG-4DCBCT$^{1200}_{-}$	RMG-4DCBCT$^{600}_{-}$
Gantry velocity	1.5°/s	Varies	Varies	Varies
Gantry acceleration	0°/s^2	Varies	Varies	Varies
Projections/bin	NA	120	120	60
Total projections	1200	1200	1200	600
Imaging time	240s	$\approx$ 240s	$120 \times \omega$	$60 \times \omega$
Relative dose	1	1	1	0.5

algorithms with the parameters used for the 4DCBCT methods summarised in Table 1. Each algorithm will be discussed in more detail below.

In the following discussion we will use the word *time window* to refer to the time between the entry and exit of a respiratory bin in a single breathing cycle. Each respiratory bin is made up of a number of time windows; one time window for each breathing cycle. Unless the gantry is moving rapidly, if multiple projections are acquired in a time window the projections are likely to be clustered together.

3.1. Conventional 4DCBCT

The conventional 4DCBCT algorithm is used to simulate current generation 4DCBCT devices. In current generation commercial systems the gantry is rotated at around 1.5°/s, taking 240 seconds to complete one full revolution of the patient. A projection pulse rate of between 5Hz-10Hz is commonly employed. We will use a pulse rate of 5Hz, or, 0.2 seconds in this study for a total of 1200 projections. Using conventional

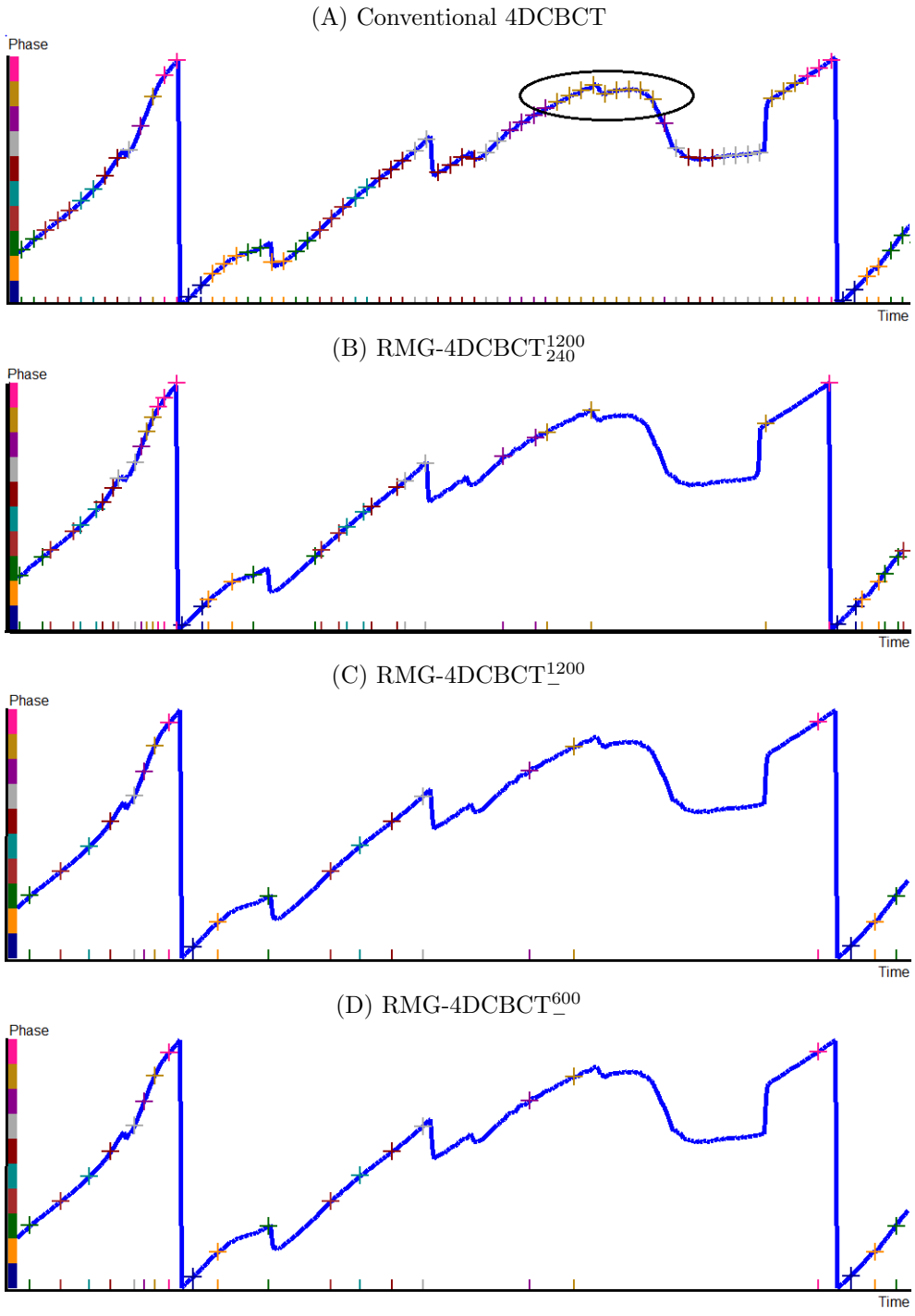

Figure 6. Screen shots of the four different 4DCBCT algorithms studied over a 15 second time period. The coloured marks on the x-axis, and the associated coloured crosses on the breathing signal represent the 10 phase bins. (A) Conventional 4DCBCT: constant gantry velocity 4DCBCT collecting 1200 projections in 240 seconds. This example gives a worst case scenario with a cluster of 9 consecutive projections in one bin. (B) RMG-4DCBCT$^{1200}_{240}$: RMG-4DCBCT collecting 120 projections per bin in 240 seconds. (C) RMG-4DCBCT$^{1200}_{-}$: RMG-4DCBCT collecting 120 projections per bin in 120 respiratory cycles. (D) RMG-4DCBCT$^{600}_{-}$: RMG-4DCBCT collecting 60 projections per bin in 60 respiratory cycles.

4DCBCT, we expect to see projection clustering as multiple projections are acquired in each time window. This is demonstrated in Figure 6A where we have marked a region where 9 consecutive projections are taken in a single time window.

3.2. RMG-4DCBCT$_{240}^{1200}$

Figure 6B demonstrates RMG-4DCBCT$_{240}^{1200}$ which attempts to acquire 1200 projections in 240 seconds; the same number of projections as for conventional 4DCBCT. Some level of projection clustering is expected with RMG-4DCBCT$_{240}^{1200}$ because a patient with a 4 second breathing cycle will acquire, on average, 2 projections per time window. When comparing conventional 4DCBCT to RMG-4DCBCT$_{240}^{1200}$ it is important to remember that there are two significant differences: (1) RMG-4DCBCT$_{240}^{1200}$ will acquire 120 projections per respiratory bin, conventional 4DCBCT rarely acquires the same number of projections in each respiratory bin, (2) RMG-4DCBCT is based on a representative breathing trajectory, so if the patient breaths faster, or slower, then image acquisition will take less, or more, than 240 seconds respectively.

3.3. RMG-4DCBCT$_{-}^{1200}$

The remaining variations of the RMG-4DCBCT algorithm collect only one projection in each time window. We use RMG-4DCBCT$_{-}^{1200}$ to represent the case where one projection is taken in each time window with the aim of collecting 120 projections per respiratory bin. This requires a total of 120 respiratory cycles per patient. For a patient with a 4 second breathing period this will take at least 480 seconds. Figure 6C demonstrates this method of acquisition in more detail. We expect very good projection separation but increased image acquisition time.

3.4. RMG-4DCBCT$_{-}^{600}$

One of the aims of RMG-4DCBCT is to reduce the imaging dose to the patient. With better projection separation there is no need to acquire 120 projections per respiratory bin. RMG-4DCBCT$_{-}^{600}$ represents the case where we only acquire 60 projections per respiratory bin in 60 breathing cycles. This is likely to halve the imaging time and radiation dose when comparing RMG-4DCBCT$_{-}^{1200}$ to RMG-4DCBCT$_{-}^{600}$.

3.5. Lung Cancer Patient Breathing Traces

We use the 112 free breathing traces from 24 lung cancer patients from a study at Virginia Commonwealth University (VCU) (George et al. 2006). We have performed a variety of simulations using different values of maximum velocity, acceleration and imaging frequency with the values summarised in Table 2.

Table 2. Maximum velocity, acceleration and imaging frequency used in RMG-4DCBCT simulations. It should be noted that only the values in the three rows are available mechanically possible on existing linac based 4DCBCT systems.

Simulation Name	Max Hz	Max Vel	Max Accel	Justification
Linac low	10	$6°/s$	$1.8°/s^2$	Velocity IEC limited. Acceleration lower limit of (Boylan et al. 2011).
Linac mid	10	$6°/s$	$4.3°/s^2$	Velocity IEC limited. Acceleration upper limit of (Boylan et al. 2011).
Linac high	10	$6°/s$	$12°/s^2$	Velocity IEC limited. Acceleration from TrueBeam.
Linac highest	10	$9°/s$	$12°/s^2$	50% increase on IEC velocity. Acceleration from TrueBeam.
C-arm	80	$100°/s$	$200°/s^2$	Kuka robot mounted Siemens Zeego.

3.6. Projection clustering metrics

The primary projection clustering metric is the RMS as defined by equation 2 with a smaller value indicating better image quality. We average the RMS for each simulation across the 112 breathing traces to generate the results in our tables. Another important metric is the number of projections collected in each respiratory bin. Conventional 4DCBCT does not guarantee 120 projections in each respiratory bin and for irregular breathers there can be a large range between the respiratory bin with the least and most projections. For RMG-4DCBCT we expect to collect 120 projections per respiratory bin, but due to the jumps in the respiratory signal, section 2.5.3, this is not always the case. For each simulation we record the respiratory bin with the fewest projections and then average this number across the 112 breathing traces. We do the same for the respiratory bin with the most projections. We record these numbers as the average minimum number of projections and the average maximum number of projections.

Although not a projection clustering metric the total imaging time, or the total time that the patient spends on the couch during imaging, is an important metric. If the imaging time is increased with RMG-4DCBCT then clinical acceptance of the method will be hindered.

3.7. Image quality metrics

To test projection clustering and the number of projections on image quality we have used the Catphan phantom to reconstruct CBCT images using Cobra¶. The reconstruction gives 160 slices (256×256 pixels per slice) spaced 1mm apart, see figure 7 for examples of the Catphan images. The Catphan phantom allows us to examine the image quality without the added complication of patient to patient variations and enables ground truth comparisons. The full data set of the Catphan phantom consists

¶ COBRA, Exxim Computing Corporation, 3825 Hopyard Road, Suite 220, Pleasanton, CA 94588

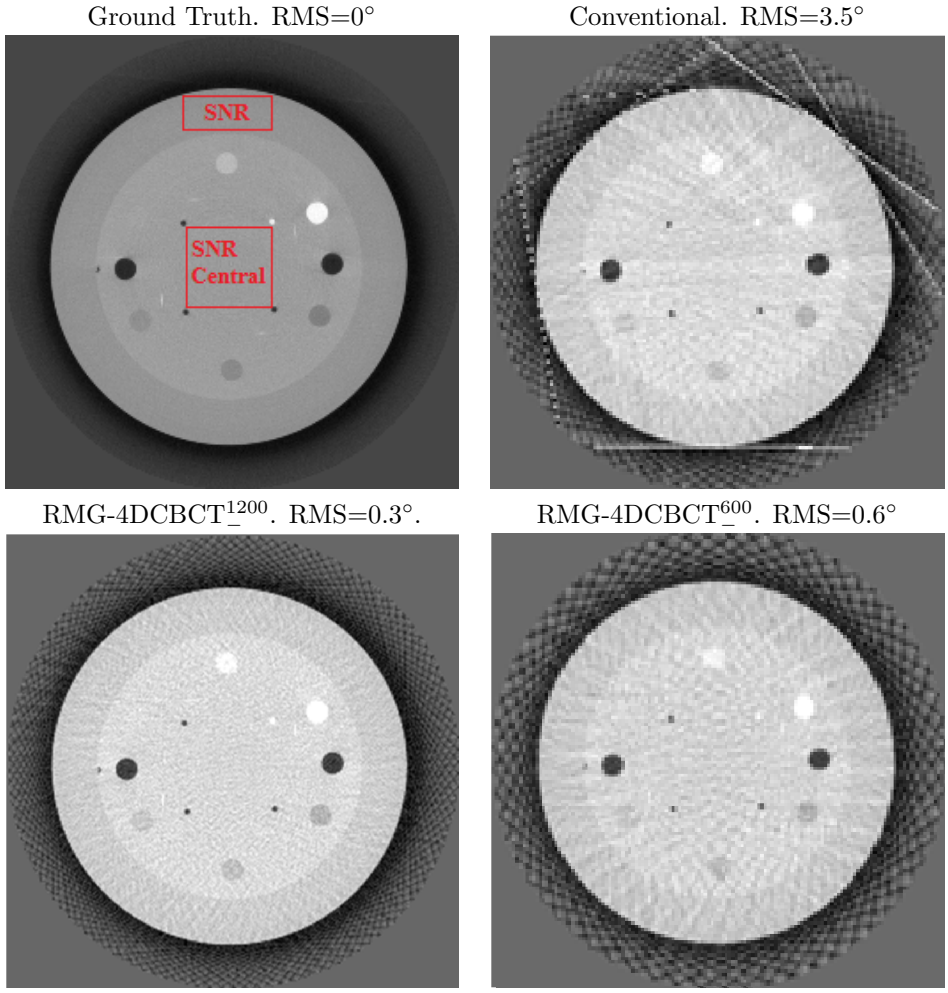

Figure 7. Reconstructed images of the Catphan phantom for the ground truth (608 projections), conventional 4DCBCT (120 projections), RMG-4DCBCT$_{-}^{1200}$ (120 projections), RMG-4DCBCT$_{-}^{600}$ (60 projections) (slice 55 is shown). The two red rectangles in the ground truth image represent the regions used to calculate the signal to noise ratio.

of 608 half fan projections which were sampled to reconstruct the images for each respiratory bin. For each projection in our simulation, the projection with the closest gantry angle from the Catphan dataset was selected. Images were then reconstructed for each of the 10 respiratory bins and each of the 112 breathing traces giving a total of 1120 CBCT reconstructions.

Our first image quality metric is the streak ratio (Leng et al. 2008). The streak ratio for a slice, i, is calculated using

$$SR_i = (TV(Image_i) - TV(GT_i))/TV(GT_i).$$

where $TV(Image_i)$ is the total variation for slice i in the reconstructed image and $TV(GT_i)$ is the total variation for slice i in the ground truth image. The average streak ratio was obtained by averaging over the 160 slices, 10 respiratory bins and 112

breathing traces (i.e. we computed the mean and standard deviation for the streak ratio over 179,200 slices).

Our second image quality metric is the signal to noise ratio, SNR. We calculate the SNR from two rectangles in slice 55 of the reconstructed Catphan image. The two rectangles are on different intensity disks in the image and are shown in Figure 7. The SNR is calculated by dividing the mean intensity by the standard deviation of the intensities of the pixels in each rectangle. A higher value indicates better image quality. The SNR calculation was performed for the 10 respiratory bins and 112 breathing traces to give 1120 SNR values from which the mean and standard deviation in the SNR was calculated.

Our final image quality metric is the normalised difference. We calculate a difference image by subtracting the reconstructed image from the ground truth image. We then sum the absolute value of the pixel intensity and divide this number by the sum of the pixel intensity in the ground truth image. The normalised difference is averaged over the 10 respiratory bins and 112 breathing traces (1120 reconstructions in total) and the standard deviation in the normalised difference is calculated.

4. Results

Examples of images reconstructed using the four 4DCBCT methods are given in Figure 7. It should be noted that RMG-4DCBCT$^{600}_{_}$ was reconstructed using half the number of projections, and half the imaging dose, than conventional 4DCBCT while the image quality is similar. We will examine both the projection clustering and image quality metrics in the remainder of this section.

4.1. Projection clustering metrics

Table 3 gives a comparison of the projection clustering metrics using the linac low settings. The RMS is significantly improved for RMG-4DCBCT$^{1200}_{_}$ and RMG-4DCBCT$^{600}_{_}$ when compared to conventional 4DCBCT. However, for RMG-4DCBCT$^{1200}_{_}$ the imaging time is more than double that of conventional 4DCBCT. With both the RPM and Ruan phase, the minimum and maximum number of projections using RMG-4DCBCT has a lower spread than for conventional 4DCBCT so we expect more consistent image quality from bin to bin using RMG-4DCBCT. Using the Ruan phase, which does not have the jumps in the phase signal, the RMS for RMG-4DCBCT$^{1200}_{_}$ and RMG-4DCBCT$^{600}_{_}$ are lower than using the RPM phase indicating that the method used to calculate the real-time phase signal is important. The much larger spread between the minimum and maximum number of projections with the RPM phase signal is also caused by the jumps in the phase signal.

In Table 3 the RMS using RMG-4DCBCT$^{1200}_{240}$ is not significantly improved over conventional 4DCBCT. With RMG-4DCBCT$^{1200}_{240}$ on average two projections are required per time window and with the linac low settings for acceleration and velocity the

Table 3. Comparison between different 4DCBCT algorithms: Average of key projection clustering metrics for different 4DCBCT methods across the 112 breathing traces using linac low. These values represent a lower bound of performance that all linacs can achieve.

4DCBCT Algorithm	RMS	Imaging time (sec)	Minimum projections	Maximum projections
RPM phase				
Conventional	3.5°	240	109	134
RMG-4DCBCT$^{1200}_{-}$	0.3°	546	115	126
RMG-4DCBCT$^{600}_{-}$	0.6°	273	57	63
RMG-4DCBCT$^{1200}_{240}$	2.6°	260	111	133
Ruan phase				
Conventional	3.9°	240	81	205
RMG-4DCBCT$^{1200}_{-}$	0.0°	580	120	120
RMG-4DCBCT$^{600}_{-}$	0.0°	290	60	60
RMG-4DCBCT$^{1200}_{240}$	3.0°	243	118	122

Table 4. Comparison between different linac models: Average of key projection clustering metrics for RMG-4DCBCT$^{1200}_{240}$ across the 112 breathing traces using a variety of different linac models and the RPM phase signal.

Linac	RMS	Imaging time(sec)	Minimum projections	Maximum projections
Linac low	2.6°	260	111	133
Linac mid	2.6°	260	110	134
Linac high	2.4°	260	111	133
Linac highest	2.4°	260	111	133
C-arm 80Hz	1.1°	264	108	130

projections cannot be separated enough to reduce the RMS. Table 4 gives a comparison with different linac models using RMG-4DCBCT$^{1200}_{240}$. We can see improvements with increased acceleration of the linac. However, the improvements are small for linac highest and only become significant for the C-arm system.

As the C-arm system has a much higher imaging frequency, maximum velocity and maximum acceleration than current generation linacs, we can reduce the total imaging time required to collect 1200 projections. In Table 5 we list the projection clustering metrics using the C-arm system and different total imaging times. As we reduce the total imaging time, RMG-4DCBCT is forced to take projections closer together with a much higher gantry velocity and acceleration. As one would expect the RMS increases as the imaging time is reduced because the gantry has less time to move into position for the next projection and more projections are acquired before a jump in the real-time phase signal is detected. The high spread between the minimum and maximum projections indicates that the jumps in the RPM phase signal have a significant impact on projection acquisition and further research on real-time phase estimation will be

Table 5. Reducing the imaging time with the C-arm system: Average of key projection clustering metrics for RMG-4DCBCT$_T^{1200}$ across the 112 breathing traces using the C-arm and the RPM phase signal. T is the total time allowed in the optimisation to acquire 1200 projections.

Imaging Time (T sec)	RMS	Minimum projections	Maximum projections
240	1.1°	108	130
200	1.5°	102	137
160	1.9°	94	144
120	3.1°	95	142
80	4.7°	99	139
60	5.5°	103	136

Table 6. Image quality metrics for different 4DCBCT algorithms: Mean and standard deviation of key image quality metrics for different 4DCBCT methods across the 10 respiratory bins and 112 breathing traces (1120 reconstructions) using linac low for acceleration and velocity. The results in this table are for the same simulations as in Table 3.

4DCBCT Algorithm	Streak Ratio	Signal to noise ratio - upper	Signal to noise ratio - central	Normalised difference
RPM phase				
Conventional	5.2 ± 3.3	189 ± 55	179 ± 53	1.0 ± 0.9
RMG-4DCBCT$_{-}^{1200}$	1.6 ± 0.2	300 ± 13	291 ± 13	0.3 ± 0.0
RMG-4DCBCT$_{-}^{600}$	2.9 ± 0.9	192 ± 23	172 ± 20	0.5 ± 0.4
RMG-4DCBCT$_{240}^{1200}$	4.3 ± 2.7	194 ± 47	194 ± 47	0.7 ± 0.7
Ruan phase				
Conventional	6.5 ± 3.6	157 ± 65	152 ± 63	1.4 ± 1.1
RMG-4DCBCT$_{-}^{1200}$	1.5 ± 0.0	305 ± 5	296 ± 2	0.2 ± 0.0
RMG-4DCBCT$_{-}^{600}$	2.6 ± 0.0	200 ± 4	179 ± 3	0.4 ± 0.0
RMG-4DCBCT$_{240}^{1200}$	4.2 ± 2.8	206 ± 49	197 ± 48	0.7 ± 0.7

necessary if C-arm systems are to be used.

4.2. Image quality metrics

Although the projection clustering metrics are useful it is important to establish that a lower RMS leads to better image quality. Table 6 compares the image quality metrics for linac low with different 4DCBCT algorithms. This table confirms that the RMS is a good indicator of image quality with similar trends to those observed in Table 3 also occur in Table 6. The most significant result in Table 6 is that the signal to noise ratio for RMG-4DCBCT$_{-}^{600}$ is comparable to both conventional 4DCBCT and RMG-4DCBCT$_{240}^{1200}$. This suggests that we can achieve similar image quality with approximately half the projections.

5. Discussion and Limitations

We have simulated RMG-4DCBCT using breathing traces from 112 lung cancer patients. Our software has been designed so that once we have an imager where projection acquisition and gantry velocity can be controlled it is relatively easy to replace our simulated imager and gantry with a real imager and gantry.

We have compared RMG-4DCBCT to conventional 4DCBCT using both image quality metrics and projection clustering metrics to demonstrate that RMG-4DCBCT shows promise for improving image quality and reducing radiation dose for both current generation linear accelerators and high end 4DCBCT systems. For current generation linear accelerators the radiation dose can be halved using RMG-4DCBCT$^{600}_{-}$ for similar image quality when compared to conventional 4DCBCT. With the C-arm system, which is capable of much higher gantry acceleration and velocity, the imaging time can be reduced using RMG-4DCBCT.

Active 4DCBCT and respiratory triggered 4DCBCT have recently been published (Fast et al. 2013) and (Cooper et al. 2013) respectively. Active 4DCBCT regulates the projection pulse rate but not the gantry speed and has been experimentally implemented by (Fast et al. 2013). Respiratory triggered acquisition maintains a fixed projection pulse rate but discards, or does not take a projection, if a projection has already been acquired in the current respiratory bin (Cooper et al. 2013). The advantage in controlling the gantry for RMG-4DCBCT is that image acquisition can be completed faster with better projection clustering than methods where just the projection pulse rate are regulated.

This paper has focused on phase binning rather than displacement binning because phase binning is currently used clinically. Displacement binning suffers from baseline drifts and shallow breathing. However, in our previous study, (O'Brien et al. 2013), we demonstrated that displacement binning has the potential to reduce the total imaging time and improve projection clustering in comparison to phase binning. Overcoming the problems mentioned above with displacement binning would be an advantage for 4D acquisition in general.

The main limitation of RMG-4DCBCT is that it puts more emphasis on real-time estimation of the phase. Although we have demonstrated that the Ruan phase produces a smooth phase signal, the Ruan phase has not been tested clinically. More work on real-time phase estimation is necessary if phase based binning is to be used clinically.

It was demonstrated by (O'Brien et al. 2013) using a more complicated heuristic solution method to compute the gantry trajectory and projection pulse rate interval, that better gantry trajectories are available when the gantry acceleration and velocity are high (e.g. for the C-arm system). Unfortunately, the more complicated heuristic solution method takes several days to find a better solution than the simpler heuristic solution used in this paper. Further work developing a method to optimise the gantry trajectory and projection time interval schedule would further reduce projection clustering for the C-arm system.

6. Conclusions

This is the first study to simulate RMG-4DCBCT using breathing traces from lung cancer patients. We have demonstrated that RMG-4DCBCT can be used to reduce imaging dose and improve image quality when acquiring 4DCBCT images. It has been shown that there is a trade-off between image quality, imaging dose and acquisition time that needs to be balanced for a particular application. For example, for the same image quality RMG-4DCBCT can reduce the imaging dose by up to 50% when compared to conventional 4DCBCT and for the C-arm system studied the imaging time can be reduced to as low as 60 seconds.

Acknowledgments

Professor Keall would like to acknowledge the support of a National Health and Medical Research Council (NHMRC) Australia Fellowship. This project was supported in part by NHMRC project grant 1034060.

References

Berbeco R I, Mostafavi H, Sharp G C & Jiang S B 2005 Towards fluoroscopic respiratory gating for lung tumours without radiopaque markers *Physics in Medicine and Biology* **50**(19), 4481–4490.

Boylan C J, Rowbottom C G & Mackay R I 2011 The use of a realistic VMAT delivery emulator to optimize dynamic machine parameters for improved treatment efficiency *Physics in Medicine and Biology* **56**(13), 4119–4133.

Cooper B J, O'Brien R T, Balik S, Hugo G D & Keall P J 2013 Respiratory triggered 4D cone-beam computed tomography: a novel method to reduce imaging dose *Med Phys* **40**(4), 041901.

Fast M, Wisotzky E, Oelfke U & Nill S 2013 Actively Triggered 4d Cone-Beam CT Acquisition *Medical Physics* **40**(9), 0.

Feldkamp L A, Davis L C & Kress J W 1984 Practical Cone-Beam Algorithm *Journal of the Optical Society of America a-Optics Image Science and Vision* **1**(6), 612–619.

George R, Chung T D, Vedam S S, Ramakrishnan V, Mohan R, Weiss E & Keall P J 2006 Audio-visual biofeedback for respiratory-gated radiotherapy: impact of audio instruction and audio-visual biofeedback on respiratory-gated radiotherapy *Int J Radiat Oncol Biol Phys* **65**(3), 924–33.

Kavanagh A, Evans P M, Hansen V N & Webb S 2009 Obtaining breathing patterns from any sequential thoracic x-ray image set *Physics in Medicine and Biology* **54**(16), 4879–4888.

Krauss A, Nill S & Oelfke U 2011 The comparative performance of four respiratory motion predictors for real-time tumour tracking *Phys Med Biol* **56**(16), 5303–17.

Leng S, Zambelli J, Tolakanahalli R, Nett B, Munro P, Star-Lack J, Paliwal B & Chen G H 2008 Streaking artifacts reduction in four-dimensional cone-beam computed tomography *Med Phys* **35**(10), 4649–59.

O'Brien R T, Cooper B J & Keall P J 2013 Optimizing 4D cone beam computed tomography acquisition by varying the gantry velocity and projection time interval *Phys Med Biol* **58**(6), 1705–23.

Ruan D, Fessler J A, Balter J M & Keall P J 2009 Real-time profiling of respiratory motion: baseline drift, frequency variation and fundamental pattern change *Phys Med Biol* **54**(15), 4777–92.

Sonke J J, Zijp L, Remeijer P & van Herk M 2005 Respiratory correlated cone beam CT *Medical Physics* **32**(4), 1176–1186.

Sweeney R A, Seubert B, Stark S, Homann V, Muller G, Flentje M & Guckenberger M 2012 Accuracy

and inter-observer variability of 3D versus 4D cone-beam CT based image-guidance in SBRT for lung tumors *Radiat Oncol* **7**, 81.

Taguchi K 2003 Temporal resolution and the evaluation of candidate algorithms for four-dimensional CT *Medical Physics* **30**(4), 640–650.

Van Herk M, Zijp L, Remeijer P, Wolthaus J & Sonke J 2007 On-line 4D cone beam CT for daily correction of lung tumour position during hypofractionated radiotherapy *International conference on the Use of Computer in Radiation Therapy* .

Vergalasova I, Cai J & Yin F F 2012 A novel technique for markerless, self-sorted 4D-CBCT: Feasibility study *Medical Physics* **39**(3), 1442–1451.

Zijp L, Sonke J & Herk M 2004 Extraction of the respiratory signal from sequential thorax cone-beam X-ray images. *International conference on the Use of Computer in Radiation Therapy* pp. 507–509.